

Direct measurement of standing evanescent waves with a photon-scanning tunneling microscope

Alfred J. Meixner, Martin A. Bopp, and Guido Tarrach

We present a detailed analysis of a standing evanescent wave that is caused by total internal reflection of an Ar-ion laser beam on a glass prism and investigate the coupling to a subwavelength dielectric tip of a photon-scanning tunneling microscope that is raster scanned at a close distance over the prism surface. The intensity of the evanescent field is spatially modulated with a period of 239.2 nm. It decays exponentially with a constant of 103.9 nm with increasing distance from the prism surface. Precise measurements of the standing evanescent wave can be used to calibrate the scanner and permit one to determine the spatial resolution and the coupling efficiency of the tip.

1. Introduction

In recent years different schemes for superresolution optical microscopes (SROM's) have been realized^{1,2} that make it possible to record optical images of surfaces with visible light at a spatial resolution well below Abbé's diffraction limit of about half of a wavelength. One can achieve this by raster scanning a small aperture of subwavelength diameter in close proximity over the sample surface. Either the aperture can act as a miniature light source when it is illuminated from the back side or it can be a small probe, collecting light from the optical near field in the immediate proximity of the sample. The amount of light that couples through the aperture sensitively depends on its diameter and its distance from the surface and on the local optical properties of the sample.

The principle of the SROM was first proposed in 1928 by Synge³ and experimentally demonstrated in 1972 by Ash and Nicholls⁴ in the microwave region with a spatial resolution of $\lambda/60$. In the optical regime the feasibility of the SROM was first demonstrated independently by Pohl *et al.*⁵ and by Lewis *et al.*⁶ Since then several different types of near-field optical probes have been developed.⁷⁻¹⁰ Often the endface of a tapered optical fiber or a micropipette

serves as a nanometer-sized aperture, and a lateral resolution of 12 nm has been reported recently.¹¹ Such a high resolution can be achieved by scanning electron microscopes, electron scanning tunneling microscopes, and scanning force microscopes. However, the use of visible light adds an important new aspect to scanning probe microscopy: Wavelength-specific¹² and polarization-sensitive¹³ measurements can be performed, providing spectroscopic information about the sample with nanometer spatial resolution.

The use of an evanescent wave that is formed by total internal reflection (TIR) of a laser beam at the sample surface was introduced to the SROM by Reddick *et al.*¹⁴ and independently by Courjon *et al.*¹⁵ The evanescent wave decays from the optically denser medium (the sample) into the medium with lower refractive index (which is typically air) within only a quarter of a wavelength. The intensity of the evanescent wave is probed by means of a subwavelength dielectric tip and provides a purely optical distance control mechanism that is sensitive to local changes of the sample topography, the refractive index, and the polarization.^{16,17} This concept is called photon-scanning tunneling microscopy (PSTM) because of its similarity to the tunneling of electrons through a small gap between a conducting surface and the probing tip.

Despite the formal analogy with electron tunneling, at a surface where TIR takes place, abrupt topography or refractive-index changes always act as sources for scattering and create homogeneous waves that are not bound to the surface. The tip probes the

The authors are with the Institute of Physics, University of Basel, CH-4056 Basel, Switzerland.

Received 19 October 1993; revised manuscript received 18 April 1994.

0003-6935/94/347995-06\$06.00/0.

© 1994 Optical Society of America.

superposition of both the evanescent waves and the homogeneous waves. Particularly when the topography or the spatial variations of the refractive index have spatial frequencies that are similar to those of the homogeneous waves, intense interference patterns of homogeneous waves that dominate the optical field above the surface and significantly complicate the interpretation of the PSTM images can be present.^{16,17} However, for many applications flat samples with good surface quality can be prepared to minimize the effect of scattering and homogeneous waves.

In combination with a spectrometer, the PSTM has great potential as an analytical tool for surface spectroscopy and fluorescence microscopy, providing spectra and hence chemical information of a surface structure or a thin film with subwavelength spatial resolution.¹⁸⁻²⁰ Samples for such applications can be prepared with a very moderate roughness and generally have only small refractive-index changes that act as weak perturbations of the evanescent field. Here interference patterns of purely evanescent waves can be created on purpose in a controlled way as a means for *in situ* calibration of the scanner and the resolution of the tip in a specific measurement.

We present detailed, quantitative PSTM measurements and topographic images of standing evanescent waves bound to a high-quality glass-air boundary. Images of a plane standing evanescent wave on a prism surface have been measured previously by means of a PSTM in the visible²¹ and very recently in the near-IR region.²² Here we show how the analysis of the standing wave provides a precise calibration of the scanner and permits one to determine the resolving power and the effective collection efficiency of the tip. Moreover, such measurements are vital for the development of a theoretical understanding of the coupling mechanism between the evanescent wave and the tip.²³⁻²⁵

2. Principle of the PSTM

The optical part of the PSTM configuration is schematically shown in Fig. 1. Two counterpropagating evanescent waves are formed by total reflection of an Ar-ion laser beam inside a 90° prism, which has a reflection coating on the output face. The probing tip is brought in a controlled fashion into the optical near field by means of a four-segment piezoelectric tube scanner. The tip scatters the evanescent field and creates propagating waves that can be detected in the far field. A considerable fraction of the scattered intensity is coupled into a propagating mode of the fiber. At its end the optical power is detected by a calibrated photodiode that is connected to a picowatt optical power meter, directly providing a power measurement. The analog output is connected to a scanning tunneling microscope control unit.

We fabricated the fiber tips reproducibly by locally melting and pulling the single-mode optical fibers as described by others.¹¹ The typical fiber tips used in these experiments had a cone half-angle of ~10 deg

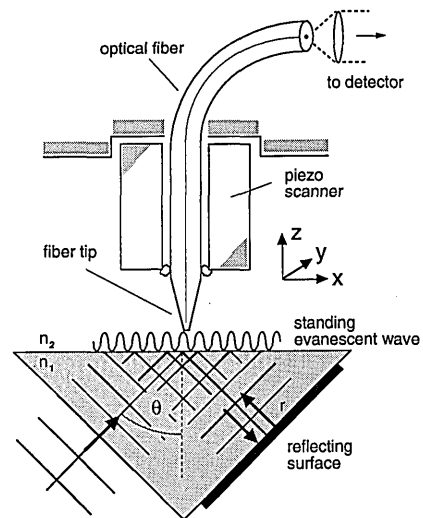


Fig. 1. Arrangement of a PSTM for collecting photons from a standing evanescent wave bound to the surface of a prism.

and a flat endface with a diameter of less than 200 nm as determined from scanning electron micrographs.

The evanescent field extends from the surface into the air only of the order of a quarter of the wavelength, and although an optical field exists in the second medium, there is no net energy flow across the boundary. Hence the unperturbed evanescent field cannot be detected by the conventional far-field technique on which the classical optical microscope is based. The electric-field strength of an unperturbed evanescent wave at a point (x, z) above the boundary can be derived from Fresnel's equations²⁶ and is given for *s* polarization by Eq. (1):

$$E(x, z) = E_0 \exp(-z/d) \exp[-i(2\pi/\lambda)x], \quad (1)$$

where

$$|E_0|^2 = \frac{4n_1^2 \cos^2 \theta}{n_1^2 - n_2^2} |E_i|^2, \quad \lambda = \frac{\lambda_0}{n_1 \sin \theta},$$

$$d = \frac{\lambda_0/n_2}{2\pi[(n_1/n_2 \sin \theta)^2 - 1]^{1/2}}.$$

In Eq. (1), E_i , λ_0 , and θ are the amplitude of the incident wave, the vacuum wavelength, and the angle of incidence, respectively; n_1 and n_2 are the indices of refraction of the optically denser medium and the optically rarer medium, respectively. The amplitude E_0 of the evanescent wave at the boundary is given by the vector sum of the electric-field amplitudes of the incident and the reflected beams. Hence the field strength of the evanescent wave at the boundary can be higher than the field strength of the incident wave, if θ is close to the critical angle. Note that there is a phase shift between the incident and the reflected waves that varies from 0° to 180°, depending on the angle of incidence. When θ equals the critical angle for TIR reflection, the phase shift is zero and E_0 is twice the amplitude of the incident wave, whereas for

$\theta = 90^\circ$ the reflected wave is 180° out of phase with respect to the incident wave and E_0 becomes zero. E_0 , the decay constant d , and the wavelength λ of the evanescent field, depend only on λ_0 , n_1 , n_2 , and θ .

A standing evanescent wave is formed by the interference of two totally reflected counterpropagating laser beams of identical wavelengths and polarized perpendicular to the plane of incidence. From Eq. (1) we can derive the intensity profile of the standing evanescent wave:

$$I(x, z) = I_0 \exp(-2z/d) \left[1 + r^2 + 2r \cos\left(\frac{2\pi}{\Lambda} x + \phi\right) \right]. \quad (2)$$

The intensity $I_0 = (c\epsilon_0/2)|E_0|^2$ can be directly related to the intensity of the incident wave by means of Eq. (1); c is the velocity of light, and ϵ_0 is the dielectric constant. The intensity profile is modulated along the x direction with a period of $\Lambda = \lambda_0/(2n_1 \sin \theta)$, which is half of the wavelength of an individual evanescent wave and the modulation depth $2r$ is given by the ratio of the electric-field components of the two counterpropagating waves. ϕ is an arbitrary phase shift.

For our experimental arrangement in which $\lambda_0 = 514.5$, $\theta = 45^\circ$, $n_1 = 1.520$, $n_2 = 1.000$, and $r^2 = 0.9$, we obtain for a standing evanescent wave $\Lambda = 239.2 \pm 0.2$ nm, $d/2 = 103.9 \pm 0.3$ nm, and $|E_0|^2 = (3.526 \pm 0.007)|E_i|^2$.

To estimate the coupling efficiency between the evanescent field and the tip, we consider a tip model based on frustrated TIR.¹⁸⁻²⁰ The tip is rigorously idealized by a semi-infinite medium with a planar boundary that is placed parallel to the prism surface. Assuming that the tip has the same refractive index as the prism, we can derive the transmission function through a gap of width d from Fresnel's equations²⁷:

$$T(z) = \frac{1 - \cos \beta}{\cosh\left(\frac{2z}{d}\right) - \cos \beta}, \quad (3)$$

where

$$\cos(\beta/2) = \frac{n_1^2 \cos(2\theta) + n_2^2}{n_1^2 - n_2^2}.$$

The mean power collected by the tip perpendicular to its effective aperture area σ is then

$$P(z) = I_i \cos \theta (1 + r^2) \sigma T(z), \quad (4)$$

where I_i is the intensity of the incident laser beam.

3. Experimental Results and Discussion

We have recorded the standing evanescent wave in two ways: in the constant intensity mode and with a constant tip-surface distance. In the first mode the tip follows the intensity variations of the field by adjusting the tip-sample gap so as to provide a

constant signal on the photodetector. The $3.8 \mu\text{m} \times 3.8 \mu\text{m}$ area in Fig. 2 shows a contour of the standing evanescent wave measured at a constant intensity. The dark fringes correspond to the minima, i.e., the nodes of the standing evanescent wave where the tip nearly touches the surface. The bright fringes represent the intensity maxima where the tip is moved away from the surface. Note that the contours of the nodes are somewhat blurred along the scan direction, because there the tip comes extremely close to the surface and occasionally becomes stuck on protrusions. At greater distances these deteriorations disappear completely.

The spatial modulation and the decay of the standing evanescent wave as a function of the tip-surface distance are shown in Fig. 3. The ordinate represents the optical power P (nW), measured at the output face of the fiber. The x axis corresponds to the movement of the tip perpendicular to the fringes at a constant height, and the z direction represents the tip-surface distance. We clearly see the sinusoidal intensity modulation of the standing evanescent wave and the decay with increasing distance from the surface. The curves on the logarithmic scale of Fig. 4(a) represent line sections through the data of Fig. 3 parallel to the z axis along an intensity maximum and along a minimum. For tip-surface distances $z > 130$ nm the signals follow an exponential decay. At closer distances the measured signals deviate from the exponential behavior because of the perturbation of the evanescent wave by the fiber tip and the finite tip diameter. However, note that the ratio A between the amplitude of the modulation and the average power is independent of z . A line section along the x axis at $z' = 100$ nm is shown in Fig. 4(b)

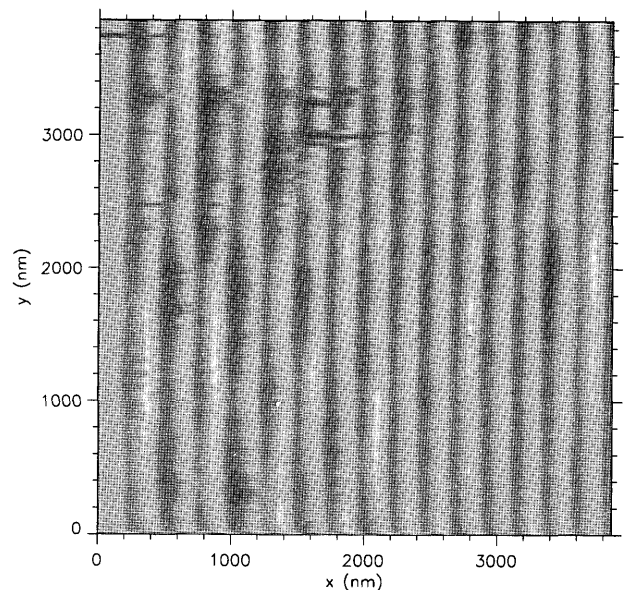


Fig. 2. Contour of the standing evanescent wave measured at constant intensity. The gray scale represents the tip-surface distance adjusted by the feedback loop. The dark fringes correspond to the nodes, and the bright fringes correspond to the intensity maxima. The period is 239.2 nm in the x direction.

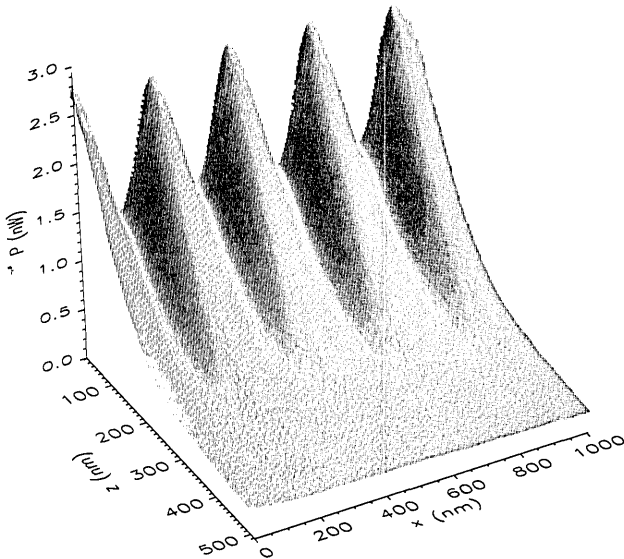


Fig. 3. Spatial modulation of the standing evanescent wave along the propagation direction of the two interfering waves (x axis) and the decay of the intensity with the increasing tip-surface distance (the z direction). The ordinate represents the optical power measured by the detector at the output face of the fiber.

and gives an experimental value of $A_{\text{exp}} = 0.33$, which is considerably less than what we expect from Eq. (2) for an unperturbed wave with $A_u = 2r/(1 + r^2) = 0.999$. This discrepancy arises from the finite effective diameter of the tip. With an infinitely small aperture one would expect the same modulation depth as in Eq. (2). As the tip diameter increases,

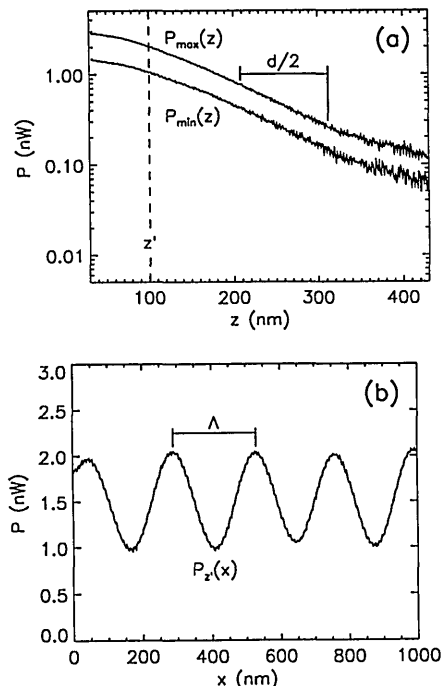


Fig. 4. (a) Line section through the data of Fig. 3 along the z direction at an intensity maximum and at a minimum. (b) Line section through the data of Fig. 3 along the x axis at a tip-surface separation of $z' = 100$ nm used for determining the effective tip diameter $\Delta = 80 \pm 1$ nm.

light is collected from a larger surface area and the spatial modulation of the signal becomes less than A_u . Modeling the collection efficiency of the fiber tip by a Gaussian probability distribution function with a cylindrical symmetry along the fiber axis and a width Δ , we can relate the amplitude of the measured signal A_{exp} to an effective aperture radius Δ :

$$A_{\text{exp}} = A_u \exp \left[- \left(\frac{\pi \Delta}{\Lambda} \right)^2 \right]. \quad (5)$$

With Eq. (5) we obtain a value of $\Delta = 80 \pm 1$ nm for a probe used for the measurements shown in Figs. 3 and 4, which is in good agreement with scanning electron micrographs of the fiber tips.

In Fig. 5 we present a global analysis of the distance dependence of coupling between the evanescent field and the tip. The dashed curve $P(z)/P_A$ was obtained by averaging the experimental data of Fig. 3 over four modulation periods along the x direction. It is normalized by the mean power P_A that would be transmitted perpendicularly through the effective aperture area σ of the tip in contact with the surface. P_A is given by $I_i \cos \theta (1 + r^2) \sigma = 3.38$ nW, where $I_i = 125$ mW/mm² is the intensity of the incident beam and $\sigma = \pi \Delta^2 = 2.0 \times 10^4$ nm² is the effective aperture area. The dotted curve is a line fit of the transmission function $\epsilon T(z - \Delta z)$ to the experimental data with the collection efficiency ϵ and the distance offset Δz as fitting parameters. For the other parameters we used the values given in Section 2 and kept them fixed for the fitting procedure. There are several points that we should note here:

- (1) For $0 < z < 325$ nm the data show an excellent fit by Eq. (3) with the decay constant $d = 103.9$ nm given by the geometry of the experimental arrangement. The coupling between the evanescent field and the tip can be nicely explained on the basis of frustrated TIR, cation, as other authors have found.²²

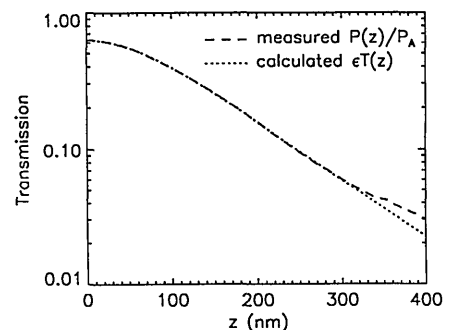


Fig. 5. Global analysis of the distance dependence of coupling between the evanescent field and the tip. The dashed curve $P(z)/P_A$ was obtained by averaging the experimental data of Fig. 3 over four modulation periods along the x direction. It is normalized by the mean power $P_A = 3.38$ nW, which would be transmitted perpendicularly through the effective aperture area σ of the tip in contact with the surface. The dotted curve is a line fit of the transmission function given in Eq. (3) to the experimental data and gives a coupling efficiency ϵ between the evanescent field and the dielectric tip of 63%.

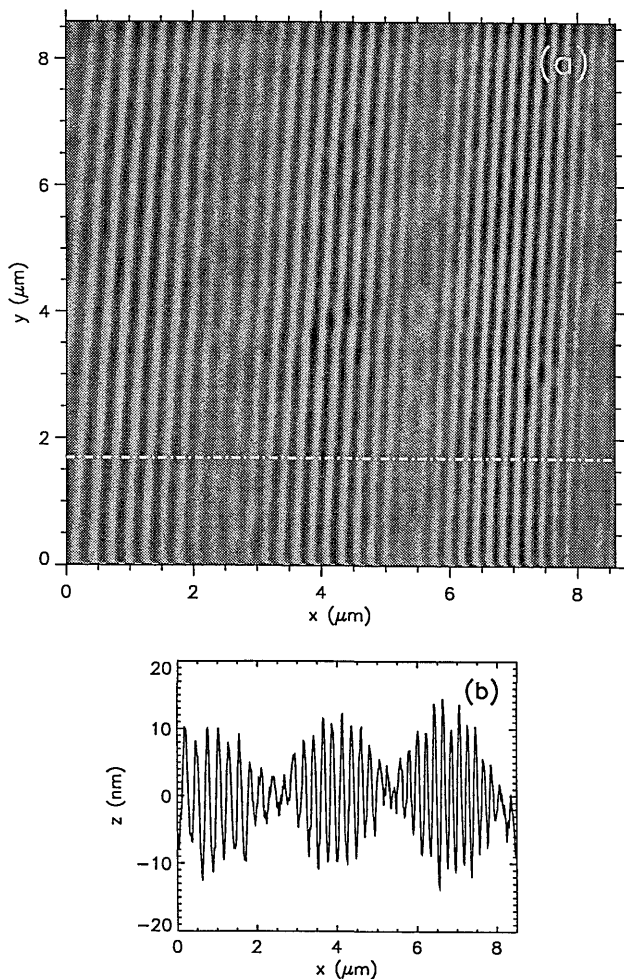


Fig. 6. (a) Operating the Ar-ion laser on all lines; the beats between the different wavelength components become visible on the standing evanescent wave. The image was recorded in the constant intensity mode with a power set point of 230 pW. (b) The section along the dashed-dot line in (a) represents the z movement of the tip adjusted by the feedback loop.

(2) The collection efficiency $\epsilon = 63\%$ is rather high. A collection efficiency of 100% could be obtained only by an infinitely extended aperture area. However, because the aperture radius $\Delta = 80 \pm 1$ nm is considerably smaller than the wavelength of the evanescent wave and the cone half-angle is only 10 deg, scattering losses at the boundary of the tip also play an important role.

(3) When the gap exceeds 325 nm, another exponential decay behavior shows up with a considerably larger decay constant of ~ 140 nm. This looks as if an additional weaker evanescent wave is present with an angle of incidence closer to the critical angle. However, extreme care has been taken to prevent beams that are backreflected from optical surfaces from reentering the prism, and so we do not understand this behavior currently.

(4) One could use the deviation from the exponential decay of the signal at close tip-surface distances for a derivative distance control at $z < 100$ nm by vibrating the fiber tip in the z direction, which would

permit determining the width of the gap without touching the surface by the tip.

So far we have discussed only standing evanescent waves caused by the interference of two counterpropagating waves of identical wavelength. Operating the Ar-ion laser on all lines leads to a standing evanescent wave that shows beats between the different wavelength components. This is demonstrated in the constant intensity measurement of Fig. 6(a) where a $8.5 \mu\text{m} \times 8.5 \mu\text{m}$ section of such a wave is shown. The z movement of the fiber tip along the x direction is represented in Fig. 6(b); it is of the order of ± 12 nm at the maxima of the beats and ± 3 nm at the nodes. The wide z dynamics leads to a much better signal-to-noise ratio than can be obtained by the constant height mode. The noise is less than 1 nm. A closer inspection reveals perturbations of the evanescent wave that are caused by variations of the surface topography, e.g., scratches, of several nanometers on the prism surface.

4. Conclusions

In summary, we have shown that the intensity profile of a standing evanescent wave of visible light with a modulation period of 239.2 nm can be measured directly with a subwavelength spatial resolution by means of a small dielectric tip of the PSTM.

Given a high-quality prism surface, a standing evanescent wave has a well-defined intensity profile, and no additional radiating modes exist as opposed to the conventional way of using holographic grating structures for determining the resolution of collection-mode near-field optical microscopes. Thus a standing evanescent wave can serve as an ideal standard for the *in situ* calibration of the scanner, the effective aperture diameter, and the collection efficiency of the near-field optical probe. For tips with an aperture diameter of 120–220 nm, we found an amazingly high coupling efficiency. This is vital for spectroscopic applications of PSTM, particularly for detecting the weak fluorescence signal from single excited dye molecules on a nanometer scale. The possibility of selectively detecting photons from a volume element with a dimension well below the optical wavelength permits one to investigate optical phenomena from a radically new point of view and provides a new source in the search of novel quantum optical phenomena.

Financial support by the Swiss Optics Priority Program, the Schweizerischer Nationalfonds, and the Treubel Fonds Basel is gratefully acknowledged. We thank I. Zschokke-Gränacher and H.-J. Güntherodt for support and stimulating discussions. Finally we thank Brugg Telecom AG for providing the single-mode optical fibers.

References

1. D. W. Pohl, "Scanning near-field optical microscopy (SNOM)," *Adv. Opt. Electron Microsc.* **12**, 243–312 (1991).
2. E. Betzig and J. K. Trautman, "Near-field optics: microscopy, spectroscopy, and surface modification beyond the diffraction limit," *Science* **257**, 189–195 (1992) and references therein.

3. E. H. Synge, "A suggested method for extending microscopic resolution into the ultra-microscopic region," *Philos. Mag.* **6**, 356–362 (1928).
4. E. A. Ash and G. Nicholls, "Super-resolution aperture scanning microscope," *Nature (London)* **237**, 510–512 (1972).
5. D. W. Pohl, W. Denk, and M. Lanz, "Optical stethoscopy: image recording with resolution $\lambda/20$," *Appl. Phys. Lett.* **44**, 651–653 (1984).
6. A. Lewis, M. Isaacson, A. Harootunian, and M. Muray, "Development of a 500 Å spatial resolution light microscope," *Ultramicroscopy* **13**, 227–231 (1984).
7. E. Betzig, M. Isaacson, and A. Lewis, "Collection mode near-field scanning optical microscopy," *Appl. Phys. Lett.* **51**, 2088–2090 (1987).
8. R. Kopelman, K. Lieberman, A. Lewis, and W. Tan, "Evanescent luminescence and nanometer-size light source," *J. Luminesc.* **48–49**, 871–875 (1991).
9. N. Kuck, K. Lieberman, A. Lewis, and A. Vecht, "Visible electroluminescent subwavelength point source of light," *Appl. Phys. Lett.* **61**(2), 139–141 (1992).
10. E. Betzig, J. K. Trautman, J. S. Weiner, T. D. Harris, and R. Wolfe, "Polarization contrast in near-field scanning optical microscopy," *Appl. Opt.* **31**, 4563–4568 (1992).
11. E. Betzig, J. K. Trautman, T. D. Harris, J. S. Weiner, and R. L. Kostelak, "Breaking the diffraction barrier: optical microscopy on a nanometric scale," *Science* **251**, 1468–1470 (1991).
12. D. Birnbaum, S.-K. Kook, and R. Kopelman, "Near-field scanning optical spectroscopy: spatially resolved spectra of microcrystals and nanoaggregates in doped polymers," *J. Phys. Chem.* **97**, 3091–3094 (1993).
13. E. Betzig, J. K. Trautman, J. S. Weiner, T. D. Harris, and R. Wolfe, "Polarization contrast in near-field scanning optical microscopy," *Appl. Opt.* **31**, 4563–4568 (1992).
14. R. C. Reddick, R. J. Warmack, and T. L. Ferrell, "New form of scanning optical microscopy," *Phys. Rev. B* **39**, 767–770 (1989).
15. D. Courjon, K. Sarayeddine, and M. Spajer, "Scanning tunneling optical microscopy," *Opt. Commun.* **71**, 23–28 (1989).
16. N. F. van Hulst, F. B. Segerink, F. Achten, and B. Bölger, "Evanescent-field optical microscopy: effects of polarization, tip shape and radiative waves," *Ultramicroscopy* **42–44**, 416–421 (1992).
17. T. L. Ferrell, J. P. Goudonnet, R. C. Reddick, S. L. Sharp, and R. J. Warmack, "The photon scanning tunneling microscope," *J. Vac. Sci. Technol. B* **9**, 525–530 (1991).
18. P. J. Moyer, C. J. Jahncke, M. A. Paesler, R. C. Reddick, and R. J. Warmack, "Spectroscopy in the evanescent field with an analytical photon scanning tunneling microscope," *Phys. Lett. A* **145**, 343–347 (1990).
19. M. A. Paesler, P. J. Moyer, C. J. Jahncke, C. E. Johnson, R. C. Reddick, R. J. Warmack, and T. L. Ferrell, "Analytical photon scanning tunneling microscopy," *Phys. Rev. B* **42**, 6750–6753 (1990).
20. S. L. Sharp, R. J. Warmack, J. P. Goudonnet, I. Lee, and T. L. Ferrell, "Spectroscopy and imaging using the photon scanning-tunneling microscope," *Acc. Chem. Res.* **26**, 377–382 (1993).
21. R. C. Reddick, R. J. Warmack, D. W. Chilcott, S. L. Sharp, and T. L. Ferrell, "Photon scanning tunneling microscopy," *Rev. Sci. Instrum.* **61**, 3669–3677 (1990).
22. F. De Fornel, E. Lesniewska, L. Salomon, and J. P. Goudonnet, "First images obtained in the near infrared spectrum with the photon scanning tunneling microscope," *Opt. Commun.* **102**, 1–5 (1993).
23. D. Van Labeke and D. Barchiesi, "Probes for scanning tunneling optical microscopy: a theoretical comparison," *J. Opt. Soc. Am. A* **10**, 2193–2201 (1993).
24. D. Barchiesi and D. Van Labeke, "Application of Mie scattering of evanescent waves to scanning tunnelling optical microscopy theory," *J. Mod. Opt.* **40**, 1239–1254 (1993).
25. L. Salomon, F. De Fornel, and J. P. Goudonnet, "Sample-tip coupling efficiencies of the photon-scanning tunneling microscope," *J. Opt. Soc. Am. A* **8**, 2009–2015 (1991).
26. M. Born and E. Wolf, *Principles of Optics* (Pergamon, London, 1975), Chap. 1, pp. 47–51.
27. S. Zhu, A. W. Yu, D. Hawley, and R. Roy, "Frustrated total internal reflection: a demonstration and review," *Am. J. Phys.* **54**, 601–607 (1986).